Stefano Bellucci (Ed.)

Physical Properties of Ceramic and Carbon Nanoscale Structures

The INFN Lectures, Vol. II

Springer

Editor
Stefano Bellucci
Istituto Nazionale di Fisica Nucleare
Laboratori Nazionali di Frascati
via E. Fermi 40
00044 Frascati RM
Italy
stefano.bellucci@lnf.infn.it

Nanotribology of Spiderman

Nicola M. Pugno

Abstract Spiders can produce cobwebs with high strength to density ratio and surprisingly display self-cleaning, strong and releasable adhesion (as geckos). Nanointerlocking, capillary and van der Waals forces, all potential adhesive mechanisms, were thus discussed, demonstrating the key role played by hierarchy to the design of super-hydrophobic, i.e. self-cleaning (by activating fakir drops as in lotus' leaves) and super-adhesive materials. The reversibility of the strong attachment was quantified thanks to an improved nonlinear peeling model, for which the solution in closed form was provided. Thus, mimicking Nature, thanks to carbon nanotube-based technology, we have suggested [N. Pugno, J. Phys. Condens. Matter **19**, 395001 (2007)] the feasibility of large invisible cables, as well as of self-cleaning, super-adhesive and releasable hierarchical smart materials. We have found that a man can be supported by a transparent cable with cross-section of 1 cm^2 and feasibly, with spider material gloves and boots, could remain attached even to a ceiling: a preliminary step towards a Spiderman suit.

Introduction

The gecko's ability to 'run up and down a tree in any way, even with the head downwards' was firstly observed by Aristotle, almost twenty-fifth centuries ago, in his *Historia Animalium*. A comparable 'adhesive' system is found in spiders, that in addition have the ability of producing fascinating cobwebs.

In general, when two solid (rough) surfaces are brought into contact with each other, physical/chemical/mechanical attractions occur (see [1]). The force developed that holds the two surfaces together is known as adhesion. Nanointerlocking

N.M. Pugno (✉)

Department of Structural Engineering, Politecnico di Torino, Corso Duca degli Abruzzi 24, 10129 Torino, Italy

e-mail: nicola.pugno@polito.it

(or friction), intermolecular forces, including capillary and van der Waals forces, suction, secretion of sticky fluids and electrostatic attraction are all potential adhesive mechanisms in biological attachment systems (see the review by [2]).

Suction cups operate under the principle of air evacuation, i.e., when they come into contact with a surface, air is forced out of the contact area, creating a pressure differential. The adhesive force generated is simply the pressure differential multiplied by the cup area. Thus, in our (sea level) atmosphere the achievable suction strength is $\sigma_s \approx 0.1$ MPa, of the same order of magnitude of those observed in the other mentioned adhesive mechanisms or in spider/gecko adhesion. Even if suction can have an interesting role in producing synthetic adhesive materials, especially to be used in high-pressure environments, its mechanics is rather trivial. Moreover, although several insects and frogs rely on sticky fluids to adhere to surfaces, synthetic materials cannot evidently secrete these fluids without uncomfortable reservoirs. Furthermore, electrostatic attraction occurs only when two dissimilar heteropolar surfaces come in close contact. Accordingly, we will omit in our discussion these three mechanisms.

In geckos the main adhesive mechanisms are capillary [3] and van der Waals [4] forces, whereas in spiders [5], in addition to the main van der Waals adhesion, nanointerlocking could have a role (e.g., during cobweb gripping). Accordingly, in this paper, we focus our attention on these three adhesive mechanisms, with an eye to the role played by hierarchy and to reversibility.

Hierarchical miniaturized hairs without adhesive secretions are characteristic features of both spiders and geckos, see Fig. 1. In jumping spider *evarcha arcuata* [5], in addition to the tarsal claws (hooks with radius of ∼50 μm), a scopula (with surface area of 37,000 μm^2) is found at the tip of the foot; the scopula is differentiated in setae, each of them covered with numerous setules (with an average density of ∼2.1 μm^{-2},) terminating in a triangular contact (with surface area of ∼0.17 μm^2.) The total number of setules per foot can be calculated at 78,000 and thus all 8 feet are provided with a total of ∼0.6 million points of contacts. The average adhesion force per setule was measured to be ∼41 nN, corresponding for the 8 feet or scopulae to $\sigma_{spider} \approx 0.24$MPa and to a safety factor, that is the adhesive force over the body weight (∼15.1 mg), of $\lambda_{spider} \approx 173$.

Similarly, a tokay gecko (*gecko gecko*) foot consists of lamellae (soft ridges ∼1 mm in length), from which tiny curved setae (∼10 μm in diameter, density of ∼0.014 μm^{-2}) extend, each of them composed by numerous spatulae (100–1,000 per seta, ∼0.1 μm in diameter) with terminal contact units (having surface area of ∼0.1 μm^2) [6, 7]. The adhesive force of a single seta and even of a single spatula has recently been measured to be respectively ∼194 μN [8] or ∼11 nN [9]. This corresponds to an adhesive strength of $\sigma_{gecko} \approx 0.58$ MPa [8] and a safety factor of $\lambda_{gecko} \approx 102$ (to compute this value we have assumed a weight of ∼250 g and a single foot surface area of ∼110 mm^2), comparable only with those of spiders (∼173 [5]), cocktail ants (>100, [10]) or knotgrass leaf beetles (∼50, [11]).

Note that such safety factors are ideal and thus are expected to be reduced by about one order of magnitude [12] as a consequence of the presence of 'defects' e.g. spurious particles, located at the contact interfacial zone. According to the previous
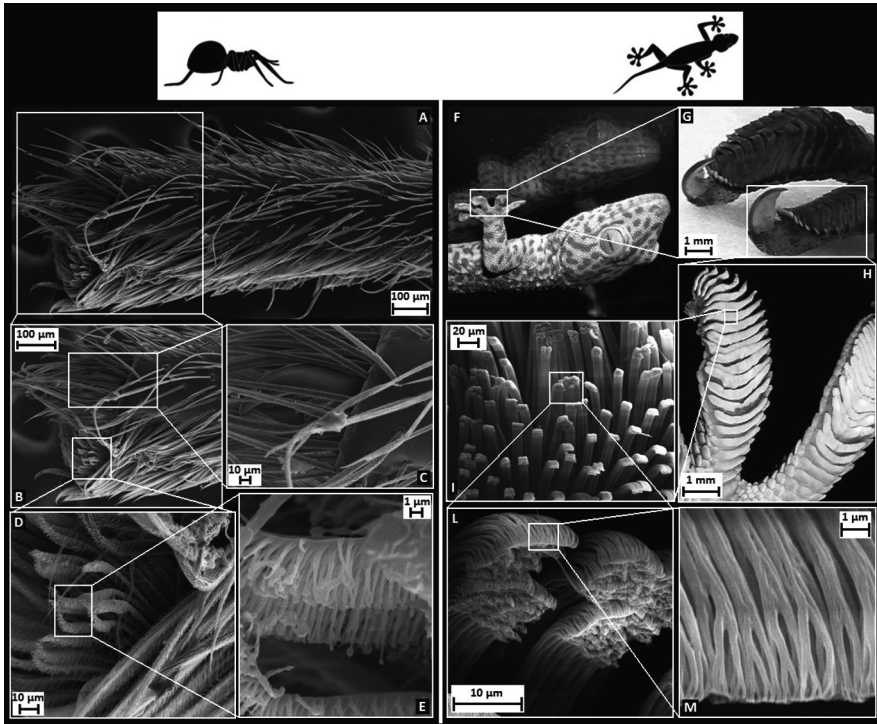
Fig. 1 Spider and gecko feet showed by SEM. In the Tokay gecko (Fig. 1f) the attachment system is characterized by a hierarchical hairy structures, which starts with macroscopic lamellae (soft ridges ∼1 mm in length, Fig. 1h), branching in setae (30–130 µm in length and 5–10 µm in diameter, Fig. 1i,l; [5, 69–71]. Each seta consists of 100–1,000 substructures called spatulae [5, 69], the contact tips (0.1–0.2 µm wide and 15–20 nm thick, Fig. 1M; [5, 69] responsible for the gecko's adhesion. Terminal claws are located at the top of each singular toe (Fig. 1g). Van der Waals and capillary forces are responsible for the generated adhesive forces [36, 72] whereas claws guarantee an efficient attachment system on surfaces with very large roughness. Similarly, in spiders (e.g. *Evarcha arcuata*, [73]) an analogous ultrastructure is found. Thus, in addition to the tarsal claws, which are present on the tarsus of all spiders (Fig. 1c), adhesive hairs can be distinguished in many species (Figs. 1d, e). Like for insects, these adhesive hairs are specialised structures that are not restricted only to one particular area of the leg, but may be found either distributed over the entire tarsus, as for lycosid spiders, or concentrated on the pretarsus as a tuft (scopula) situated ventral to the claws (Fig. 1a, 1b), as in the jumping spider *Evarcha arcuata* [73]

values, we estimate for a gecko a total number of points of contacts of ∼3 billions, thus much larger than in spiders, as required by their larger mass (the number of contacts per unit area must scale as the mass to 2/3, see [13]). The total adhesive force could easily be overcome by subsequently detaching single setules and not the whole foot at once [14, 15].

Moreover several natural materials exhibit super-hydrophobicity, with contact angles between 150° and 165°; often a strategy for allowing a safe interaction with

water. This is the case for the leaves of about 200 plants, including asphodelus, drosera, eucalyptus, euphorbia, ginkgo biloba, iris, tulipa and, perhaps the most famous, lotus [16, 17]. Similarly, animals can be super-hydrophobic, as for the case of water strider legs, butterfly wings, duck feathers and bugs [18–20]. These surfaces are generally composed of intrinsic hydrophobic material and $N=2$ hierarchical micro-sized levels [21].

Superhydrophobia is extremely important in micro/nano-fluidic devices for reducing the friction associated with the fluid flow, but also for self-cleaning: super-hydrophobic materials are often called self-cleaning materials since drops are efficiently removed taking with them the dirty particles which were deposit on them [17, 22]. This effect is extremely important in super-adhesive materials. Hansen and Autumn [23] have proved that gecko setae become cleaner with repeated use; this is probably a consequence of the hierarchical nature of the gecko foot, as we are going to demonstrate.

A replication of the characteristics of gecko [24] or spider feet would enable the development of a self-cleaning, as the lotus leaves (see the review by [21]), super-adhesive and releasable hierarchical material and, with the conjunction of large invisible cables [25], of a preliminary Spiderman suit, see Fig. 2 (Pugno, [26, 27].

Towards a Spiderman's suit

Artificial spider silk: with transparent nanotube sheets

Self-cleaning surfaces: mimicking lotus leaves

Spider (left) or gecko (right) material gloves and boots

with hierarchically branched nanotubes

Super-adhesion controlled by the hair geometry
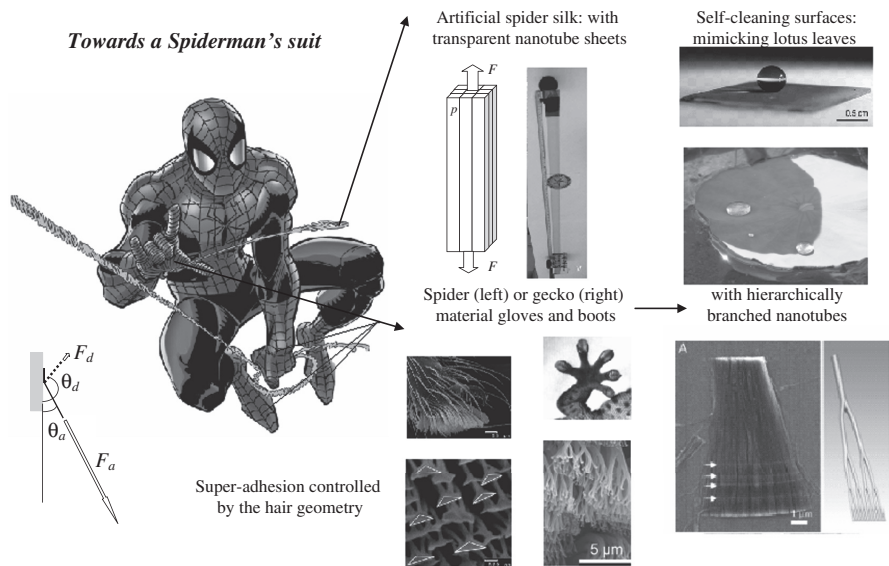
Fig. 2 Spiderman (related inset from the web) must have large cobwebs and self-cleaning, super-adhesive and releasable gloves and boots. Invisible large cables [24] could be realized with nanotube bundles (related inset from [27]), whereas gloves and boots, mimicking spider (related inset from [4]) or gecko (related inset from [50]) materials, with hierarchically branched nanotubes (related inset from [64]) as suggested by our analysis. Note that nanotube forest is super-hydrophobic (water repellent) and thus self-cleaning (related inset from [74]) as lotus leaves (related inset: photo by the Author)

Invisible Macroscopic Spider Silk

In this section we present just an idea, no more no less, for realizing large invisible cables [25]; a discussion on their technological feasibility is also included. The strength, stiffness and density of the invisible cable are estimated, and the condition of invisibility is provided.

Consider a rectangular cable having width W, thickness T and length L; the cross-section being composed of $n \times m$ (multiwalled) carbon nanotubes with inner and outer diameter d_- and d_+ respectively and length L. Let us assume that they are arranged in a square lattice with periodic spacing $p=W/n=T/m$ (see Fig. 2, related inset). Then, the strength σ_C of the bundle, defined as the failure tensile force divided by the nominal area $W \times T$, is predicted as:

$$\sigma_C = \frac{\pi}{4} \frac{d_+^2 - d_-^2}{p^2} \sigma_{NT}, \quad \sigma \to E, \rho \tag{1}$$

where σ_{NT} denotes the strength of the single carbon nanotube. To derive Eq. 1 we have assumed a full transfer load between the nanotube shells, which seems to be plausible if intertube bridgings are present, otherwise σ_{NT} would represent the nominal multiwalled nanotube strength. The same relationship is derived for the cable Young's modulus E_C considering in Eq. 1 the substitution $\sigma \to E$ and E_{NT} as the Young's modulus of the single carbon nanotube. Similarly, the cable density ρ_C, defined as the cable weight divided by the nominal volume $W \times T \times L$, is predicted according to Eq. 1 with the substitution $\sigma \to \rho$, where ρ_{NT} would denote the carbon (nanotube) density. Thus, the same (failure) strain $\varepsilon_C = \sigma_C/E_C = \sigma_{NT}/E_{NT}$ and strength over density ratio $\sigma_C/\rho_C = \sigma_{NT}/\rho_{NT}$ is expected for the bundle and for the single nanotube. This ratio is huge, at least theoretically, e.g., as required in the megacable of the space elevator [12]. Thus, Eq. 1 is a law to connect the nanoscale properties of the single nanotube with the macroscopic properties of the bundle.

On the other hand, indicating with λ the light wavelength, the condition for a nanotube to be invisible is:

$$d_+ << \lambda \tag{2a}$$

whereas to have a globally invisible cable, we require in addition to not have interference between single nanotubes, i.e.:

$$p >> \lambda \tag{2b}$$

We do not consider here the less strict limitations imposed by the sensitivity of the human eye, that can distinguish two different objects only if their angular distance is larger than ~1′. In other words, we want the cable to be intrinsically invisible.

Note that in the case of $p << \lambda$ a transparence is still achievable considering a sufficient thin sheet, as suggested by classical aerosol mixtures (here not applicable).

Assuming $d_+/\lambda \approx 1/10$, $p/\lambda \approx 10$, from the theoretical strength, Young's modulus and density of a single nanotube, we derive the following wavelength-independent invisible cable properties:

$$\sigma_C^{(theo)} \approx 10\,\text{MPa}, \quad E_C \approx 0.1\,\text{GPa}, \quad \rho_C \approx 0.1\,\text{kg}\big/\text{m}^3 \tag{3}$$

Meter-long multiwalled carbon nanotube cables can already be realized [28], suggesting that our proposal could became soon technologically feasible. For such a nanostructured macroscopic cable, a strength over density ratio of $\sigma_C/\rho_C \approx 120 - 144\text{KPa}/(\text{Kg}/\text{m}^3)$ was measured, dividing the breaking tensile force by the mass per unit length of the cable (the cross-section geometry was not of clear identification). Thus, we estimate for the single nanotube contained in such a cable $\sigma_{NT} \approx 170\text{MPa}$ ($\rho_{NT} \approx 1300\,\text{Kg}/\text{m}^3$), much lower than its theoretical or measured nanoscale strength [29]. This result was expected as a consequence of the larger probability to find critical defects in larger volumes [30]. Thus, defects limit the range of applicability of long bundles based on nanotubes, e.g. reducing their strength by about one order of magnitude [12]. However, the cable strength is expected to increase with the technological advancement. The cable density was estimated to be $\rho_C \approx 1.5\text{Kg}/\text{m}^3$ [28], thus resulting in a cable strength of $\sigma_C \approx 200\,\text{KPa}$. Note that a densified cable with a larger value of $\sigma_C/\rho_C \approx 465\,\text{KPa}/(\text{Kg}/\text{m}^3)$ was also realized [29], suggesting the possibility of a considerable advancement for this technology in the near future. For such cables a degree of transparency was observed, confirming that our proposal is realistic. Inverting Eq. 1 we deduce for them $p \approx 260\,\text{nm}$, in good agreement with the Scanning Electron Microscope (SEM) image analysis [28]. The nanotube characteristic diameter was $d_+ \approx 10\,\text{nm}$. Considering the visible spectrum, $\lambda \approx 400 - 600\,\text{nm}$, the condition (2a) was thus satisfied, whereas the condition (2b) was not satisfied. Thus, only a partial degree of transparency was to be expected (see Fig. 2, related inset).

Moreover, multiwalled carbon nanotubes with $d_+ \approx 50\text{nm}$ ($d_- \approx 0\text{nm}$) spaced by $p \approx 5\,\mu\text{m}$ are expected to realize an invisible cable with the mechanical properties given in Eq. 3. For example, this would correspond to an invisible cable with a cross-section of 1 cm^2 and weight per unit length of only 0.01 g/m, capable of supporting the weight of a man (1,000 N). However note that defects would decrease the cable strength, e.g., by one order of magnitude [12].

The nanotubes will remain parallel satisfying the condition (2b), if the cable will work under tension. A later force at the middle of the cable will tend to compact the nanotubes and at a strain of $\varepsilon \approx 8\left(W/L\right)^2$ all of them will be in contact. Since for a cable $W/L << 1$ (e.g., 10^{-2}), a strain of the order of $\varepsilon \approx 10^{-4}$, i.e. small if compared with that at failure $\varepsilon_{NT}^{(theo)} \approx \sigma_{NT}^{(theo)}\big/E_{NT} \approx 0.1$, will activate the nanotube interaction. In such a situation the cable would 'appear' near to the point of application of the lateral force, i.e. where the condition of Eq. 2b is not locally verified, to survive by activating the interaction; this behavior could help in visualizing the cable after having trapped a victim.

Obviously, reducing the requirement of invisibility to that of (a degree of) transparency would automatically lead to strongest macroscopic synthetic cobwebs. Graded cross-links are needed in order to improve the overall bundle strength [31].

Nanohooks

In this section an estimation of the elastic strength of hooks (Fig. 3a) with friction is summarized [32], treating them as elastic arcs (see [33]). We have quantified, as the intuition and Velcro® material suggest, that hooks allow reversible strong attachment, establishing elastic-plastic or hyper-elastic behaviours as dictated by the competition between friction and large displacements [32]. In addition, size-effects suggest that nano-contacts are safer. Thus, we describe here the main results of a 'Velcro nonlinear mechanics'[32], that could have interesting applications also in different fields, as suggested by its recent observation in wood [34].

The hook elastic critical force F_h (Fig. 3b) can be estimated according to:

$$F_h \approx \frac{(\pi/2 + \varphi) EI}{\pi R^2} \tag{4}$$

where φ is the friction coefficient between hook and substrate (or loop), E is the material Young modulus, I is the cross-sectional moment of inertia and R is the hook radius. Thus, if a number of hooks per unit area $\rho_h = m/[\pi (2R)^2]$ is present, corresponding to an equivalent number m of hooks per clamp, the corresponding nominal strength will be:

$$\sigma_h = \rho_h F_h = \frac{m (\pi/2 + \varphi) EI}{4\pi^2 R^4} = \frac{m (\pi/2 + \varphi) E}{16\pi (R/r)^4} \tag{5}$$

where r is the equivalent radius (in terms of inertia) of the cross-section. For example, considering m=10, $\varphi = 0$, E=10 GPa (Young's modulus for keratin
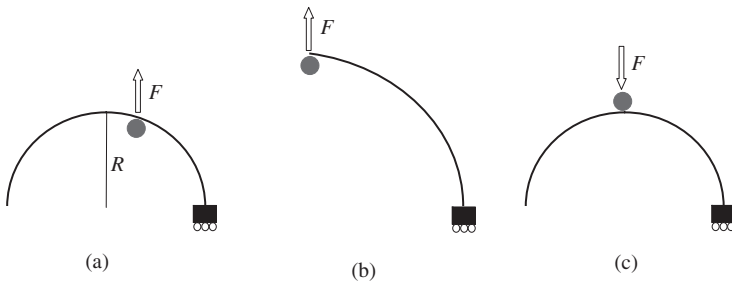

Fig. 3 Elastic hook with friction. Conditions of interlocking (**a**), ultimate "elastic" strength (**b**) and hauling (**c**)

material is $E=1\text{--}20$ GPa, see [35], and [36]) and $R/r = 10$ corresponds to $\sigma_h \approx 0.3$ MPa, comparable with the strength observed in *evarcha arcuata* spiders of $\sim$0.24 MPa ([5], note the two spider hooks in the related inset of Fig. 2).

On the other hand, the maximum force for hooking (Fig. 3c) is:

$$F_h^* = -\frac{\varphi EI}{R^2} \tag{6}$$

Consequently the ratio:

$$\mu = \frac{F_h}{|F_h^*|} = \frac{1}{\pi} + \frac{1}{2\varphi} \tag{7}$$

is expected to be very large ($\mu(\varphi \to 0) \to \infty$), and thus strong and 'reversible' adhesion is expected in hooked materials. This can be easily verified in our own home making experiments on Velcro materials, directly measuring μ and thus deducing the related friction coefficient φ. For example for $\mu \approx 10 - 100$, $\varphi \approx 5 \times 10^{-(2-3)}$.

If a contact area A supports the (e.g., animal body) weight W, the safety factor, i.e. the ratio between the attachment force and the weight $W = Mg = \rho Vg = \rho ALg$ (ρ is the density, g is the gravitational acceleration, V is the body volume and M its mass) is:

$$\lambda = \frac{\sigma_h A}{W} = \frac{1}{\rho g}\frac{\sigma_h}{L} \tag{8}$$

in which $L=V/A$ is a characteristic size of the supported weight. Thus, smaller is safer. For example, since we expect $L \propto M^{1/3}$, assuming $\sigma_h \approx const$, the predicted scaling is $\lambda = kM^{-1/3}$; noting that in the *evarcha arcuata* spiders [5] $\lambda_{spider} \approx 173$ and $M_{spider} \approx 15$mg we deduce $k_{spider} \approx 43\text{g}^{1/3}$. Thus for a Spiderman ($M_{man} \approx 70$ kg), defined as a man having gloves and shoes composed of spider material, we roughly (because self-similarity is assumed) expect $\lambda_{spiderman} \approx 1$. For gecko gloves, since for geckos $\lambda_{geckos} \approx 102$ and $M_{geckos} \approx 250$ g, we would deduce $k_{geckos} \approx 643\,g^{1/3}$ and thus $\lambda_{spiderman} \approx 15$. Accordingly, such gloves are sufficient to support Spiderman even on a ceiling.

The force carried by one hook scales as $F_1 \equiv F_h \propto r^4/R^2$, thus the bending, tensile, and nominal stresses in the hook must scale as $\sigma_b \propto r/R$, $\sigma_t \propto (r/R)^2$ and $\sigma_h \propto (r/R)^4$ respectively. Accordingly, size-effects can be predicted. For example, splitting up the contact into n sub-contacts, i.e., $R \to R/\sqrt{n}$, would result in a force $F_n = n^\beta F_1$ with $\beta = 0$ if $r \propto R$ but $\beta = 2$ if $r = const$. Thus, for this last case, sub-contacts are found to be stronger, even if the hook will be higher stressed and its mechanical strength will impose a lower-bound to the radius of the smallest hook. This explains why Nature uses nano-sized bio-contacts, since usually $0 < \beta < 2$, as recently discussed on the basis of contact mechanics (for which $\beta = 1/2$, see [13]). Pugno [26] has shown that this enhancement cannot continue ad infinitum. If the

hook weight is a constant fraction of the body weight, the scaling of the safety factor is $\lambda \propto r^2/R^3$, similarly to the prediction of Eq. 8.

Finally, the work of adhesion per unit area can be computed according to:

$$2\gamma_h = \rho_h \int_0^{F_h} \delta\,(F)\,\mathrm{d}F = \left(\frac{1}{2} + \kappa\right)\sigma_h \delta\,(F_h) \tag{9}$$

where $\kappa = 0$ for linear systems. For example, considering $\kappa = 0$, $\sigma_h = 0.3\,\mathrm{MPa}$ as previously computed, and $\delta\,(F_h) \approx R = 100\,\mathrm{nm}$ we get $\gamma_h \approx 0.03\,\mathrm{N/m}$, comparable with the work of adhesion observed in geckos (0.05 N/m, see [37]).

Nanohooks could be useful, in addition to classical mechanisms, in order to reduce the dramatic role played by the surface roughness, that will imply contact 'defects' during especially macroscopic adhesion.

Self-Cleaning Super-Adhesive Materials

The contact angle (Fig. 4a) between a liquid drop and a solid surface was found by Young [38] according to $\cos\theta = (\gamma_{SV} - \gamma_{SL})/\gamma_C$, where $\gamma_C \equiv \gamma_{LV}$ and the subscripts of the surface tensions describe the solid (S), liquid (L) and vapour (V) phases. Note that for $(\gamma_{SV} - \gamma_{SL})/\gamma_C > 1$ the drop tends to spread completely on the surface and $\theta = 0°$, whereas for $(\gamma_{SL} - \gamma_{SV})/\gamma_C > 1$ the drop is in a pure non-wetting state and $\theta = 180°$. According to the well-known Wenzel's model [39, 40] the apparent contact angle θ_W is a function of the surface roughness w, defined as the ratio of rough to planar surface areas, namely, $\cos\theta_W = w\cos\theta$ (Fig. 4b). The apparent contact angle varies also with the heterogeneous composition of the solid surface, as shown by Cassie and Baxter [41]. Consider a heterogeneous surface made up of different materials characterized by their intrinsic contact angles θ_i and let φ_i be the area fraction of each of the species; the individual areas are assumed to be much smaller than the drop size. Accordingly, the apparent contact angle θ_{CB} can be derived as $\cos\theta_{CB} = \sum_i \varphi_i \cos\theta_i$ [41].
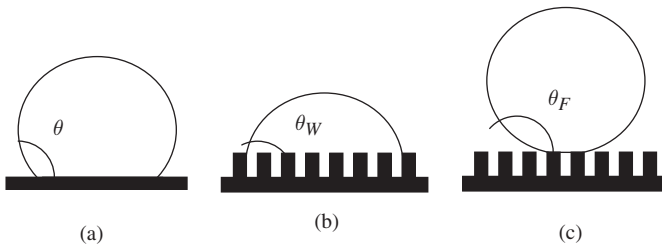

Fig. 4 Contact angles for a drop on a flat surface (**a**) or on a rough surface in the Wenzel (**b**) or Fakir (**c**) state

A droplet can sit on a solid surface in two distinct configurations or states (Fig. 4b, c). It is said to be in Wenzel state (Fig. 4b) when it is conformal with the topography. The other state in which a droplet can rest on the surface is called the Fakir state, after Quéré [42], where it is not conformal with the topography and only touches the tops of the protrusions on the surface (Fig. 4c). The observed state should be the one of smaller contact angle, as can be evinced by energy minimization [43].

Let us consider a hierarchical surface (Fig. 5). The first level is composed by pillars in fraction φ (as in Fig. 4b, c). Each pillar is itself structured in n sub-pillars in a self-similar (fractal) manner, and so on. Thus, the pillar fraction at the hierarchical level N is φ^N, whereas the related number of pillars at the level N is n^N. Applying the Cassie and Baxter law [41] for the described composite (solid/air) hierarchical surface (the contact angle in air is by definition equal to 180°) we find for the hierarchical fakir state:

$$\cos \theta_F^{(N)} = \varphi^N (\cos \theta + 1) - 1 \tag{10}$$

Note that for $N = 0$ $\cos \theta_F^{(0)} = \cos \theta$ as it must be, whereas for $N=1$ $\cos \theta_F^{(1)} = \varphi (\cos \theta + 1) - 1$, as already deduced for the case described in Fig. 4c [44]. Equation 10 quantifies the crucial role of hierarchy and suggests that hierarchical surfaces are fundamental to realize super-hydrophobic materials (effective contact angle larger than $\theta_{SHpho} \approx 150°$), since we predict $\theta_F^{(\infty)} = 180°$. The minimum number of hierarchical levels necessary to achieve super-hydrophobia in the Fakir state is thus:

$$N_{SHpho}^{(F)} = \frac{\log \left(\frac{1+\cos \theta_{SHpho}}{1+\cos \theta} \right)}{\log \varphi} \tag{11}$$

and the logarithmic dependence suggests that just a few hierarchical levels are practically required.

By geometrical argument the roughness w of the introduced hierarchical surface Fig. 5 can be calculated in closed form. The roughness at the hierarchical level k is given by $w^{(k)} = 1 + S_L^{(k)}/A$ in which A is the nominal contact area and $S_L^{(k)}$ is the total lateral surface area of the pillars. The pillar at the level k has an equivalent radius r_k and a length l_k and the pillar slenderness s, defined as the ratio between its lateral and base areas, is $s = 2l_k/r_k$. The air surface area at the level k can be computed as $A \left(1 - \varphi^k\right)$ or equivalently as $A - n^k \pi r_k^2$, thus we deduce $r_k = r_0 \left(\varphi/n\right)^{k/2}$, with $A \equiv A_0 \equiv \pi r_0^2$. Consequently:
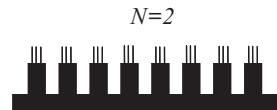
$N=2$

Fig. 5 A hierarchical surface with $N=2$ levels

$$w^{(N)} = 1 + \frac{1}{\pi r_0^2} \sum_{k=1}^{N} 2\pi r_k l_k n^k = 1 + s \sum_{k=1}^{N} \varphi^k = 1 + s \frac{\varphi - \varphi^{N+1}}{1 - \varphi} \quad \forall n \quad (12)$$

Note that the result becomes independent from n (and that $w^{(0)}(\varphi) = 1 = w^{(N)}(\varphi = 0)$, $w^{(1)} = 1 + s\varphi$, whereas $w^{(N \neq 1)}(\varphi = 1) = \infty$). Thus we find for the hierarchical Wenzel state:

$$\cos \theta_W^{(N)} = w^{(N)} \cos \theta = \left(1 + s \frac{\varphi - \varphi^{N+1}}{1 - \varphi}\right) \cos \theta \quad (13)$$

Equation 13 suggests that hierarchical surfaces can be interesting also to realize super-hydrophilic materials, since we predict $\cos \theta_W^{(\infty)} = w^{(\infty)} \cos \theta$ with $w^{(\infty)} = 1 + s\varphi/(1 - \varphi)$; thus if $\cos \theta > 0$ $\theta_W^{(\infty)} \to 0$, for $s \to \infty$ or $\varphi \to 1$. However note that for $\cos \theta < 0$, $\theta_W^{(\infty)} \to 180°$ ($s \to \infty$ or $\varphi \to 1$), and thus super-hydrophobia can take place also in the Wenzel state, without invoking fakir drops. The minimum number of hierarchical levels necessary to render the surface super-hydrophobic/hydrophilic in the Wenzel state is thus:

$$N_{SHpho, phi}^{(W)} = \frac{\log\left(1 + \frac{(1-\varphi)}{s\varphi}\left(1 - \frac{\cos \theta_{SHpho, phi}}{\cos \theta}\right)\right)}{\log \varphi} \quad (14)$$

where effective contact angles smaller than θ_{SHphi} define super-hydrophily.

Comparing $\theta_W^{(N)}$ and $\theta_F^{(N)}$, we find that the Fakir state is activated at each hierarchical level for (we omit here second order problems, related to metastability, contact angle hysteresis and limit of the Wenzel's approach, for which the reader should refer to the review by [21]):

$$\theta > \theta_{WF}, \quad \cos \theta_{WF} = -\frac{1 - \varphi^N}{w^{(N)} - \varphi^N} = -\frac{1}{w^{(\infty)}} = -\frac{1 - \varphi}{1 + \varphi(s - 1)} \quad \forall N \quad (15)$$

Note that the result is independent from N and $\theta_{WF} \to 90°$ for $s \to \infty$ or $\varphi \to 1$, and thus a hydrophobic\hydrophilic material composed by sufficiently slender or spaced pillars surely will/will not activate fakir drops and will become super-hydrophobic\hydrophilic for a large enough number of hierarchical levels. Thus hierarchy can enhance the intrinsic property of a material. The role of hierarchy is summarized in the phase diagram of Fig. 6.

For example, for plausibly values of $\varphi = 0.5$ and $s=10$ we find from Eq. 15 $\theta_{WF} = 95.2°$; thus assuming $\theta = 95°$ the Fakir state is not activated and the Wenzel state prevails (if the Fakir state still prevails it is metastable, see [21]). From Eq. 12 $w^{(1)} = 6$, $w^{(2)} = 8.5$, $w^{(3)} = 9.75$ and $w^{(4)} = 10.375$; accordingly from Eq. 13 $\theta_W^{(1)} \approx 122°$, $\theta_W^{(2)} \approx 138°$, $\theta_W^{(3)} \approx 148°$ and $\theta_W^{(4)} \approx 155°$, thus $N=4$ hierarchical levels are required for activating super-hydrophobia (from Eq. 14 $N_{SHpho}^{(W)} = 3.2$). On the other hand, assuming $\theta = 100°$ fakir drops are activated and from Eq. 10
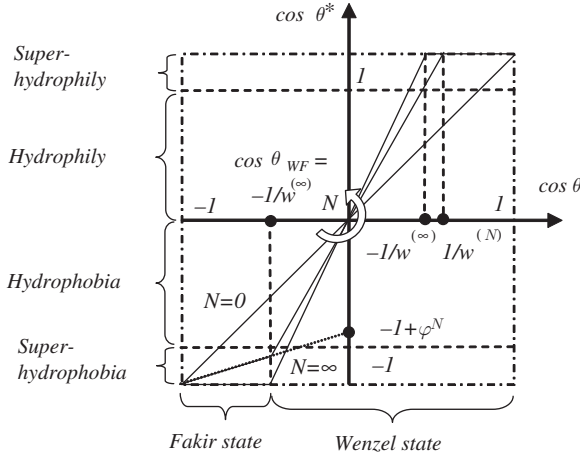
Fig. 6 Effective contact angle $\theta^* = \theta_{F,W}^{(N)}$ as a function of the intrinsic one θ by varying the number N of hierarchical levels. Thus, super-hydrophobic/hydrophilic surfaces can be obtained by an opportune design of the hierarchical architecture, according to this phase diagram and reported equations (note that metastable fakir drops could be observed also in the Wenzel region, dotted line, see [20])

$\theta_F^{(1)} \approx 126°$, $\theta_F^{(2)} \approx 143°$ and $\theta_F^{(3)} \approx 154°$, thus $N=3$ hierarchical levels are sufficient to achieve super-hydrophobia (from Eq. 11 $N_{SHpho}^{(F)} = 2.6$).

Some insects, such as the beetle *Hemisphaerota cyanea*, use capillary to stick to their substrate, generating a force close to 1 g (i.e. 60 times its body mass) for more than 2 min [45], allowing them to resist attacking ants; tokay geckos use the same principle (in addition to van der Waals forces) to generate their tremendous adhesion [3].

Between a spherical surface (contact angle θ) of radius r_0 and a flat plate (contact angle θ_P), the capillary attractive or repulsive force is predicted to be $F_C = 2\pi r_0 \gamma_C (\cos\theta + \cos\theta_P)$ [46]. Thus, for a pillar of size r_0 composed by N hierarchical levels the force is $F_C^{(N)} = n^N 2\pi r_N \gamma_C (\cos\theta + \cos\theta_P)$ and the nominal strength $\sigma_C^{(N)} = F_C^{(N)} \big/ (\pi r_0^2)$ becomes:

$$\sigma_C^{(N)} = \frac{2(\varphi n)^{N/2}}{r_0} \gamma_C \left(\cos\theta_{W,F}^{(N)} + \cos\theta_P \right) \tag{16}$$

Note that for $N=0$ such a capillary strength corresponds to the previously discussed law. For $N=1$ the strength scales as $\sqrt{n}$, in agreement with a recent discussion [14]: splitting up the contact into n sub-contacts would result in a stronger interaction (with a cut-off at the theoretical strength): smaller is stronger (see [30]). This explains the observed miniaturized size of biological contacts. Introducing the previously computed contact angle related to the hierarchical surface allows one to

evaluate the hierarchical capillary force, with or without activation of the Fakir state. Super-attraction/repulsion can thus be achieved thanks to hierarchy, since $\sigma_C^{(N)} \approx \sigma_C^{(0)} (\varphi n)^{N/2}$.

Thus, the analysis demonstrates and quantifies that super-hydrophobic/hydrophilic and simultaneously super-attractive/repulsive surfaces can be realized, mimicking Nature thanks to hierarchical architectures. Assuming $\varphi = 0.5, n=s=10$ and $\theta \approx 120°$ (as in lotus leaves), the analysis shows that fakir drops are activated and only two hierarchical levels are required to achieve super-hydrophobia ($\theta > \theta_{WF} = 95.2°, N_{SHpho}^{(F)} = 1.9; \theta_F^{(1)} \approx 139°, \theta_F^{(2)} \approx 151°$), in agreement with direct observations on super-hydrophobic plants (see our discussing in the Introduction). Simultaneously, we deduce $\sigma_C^{(1)} \approx 2.2\sigma_C^{(0)}$, $\sigma_C^{(2)} \approx 5.0\sigma_C^{(0)}$ and $\sigma_C^{(3)} \approx 11.2\sigma_C^{(0)}$, i.e. just three hierarchical levels (or even two, if $\varphi \approx 1$ and $n \approx 10$) are sufficient to enhance the capillary strength by one order of magnitude, generating super-attractive ($\sigma_C^{(0)} > 0$) or super-repulsive ($\sigma_C^{(0)} < 0$) surfaces. Thus, the analysis suggests the feasibility of innovative self-cleaning and simultaneously super-adhesive hierarchical materials, as observed in spiders and geckos.

Analogously, hierarchy simultaneously enhances the work of adhesion, and thus the corresponding force, per unit nominal area, due to the larger effective surface area. Accordingly, the maximum (assuming all the surfaces in contact) effective work of adhesion can be derived by the following energy equivalence:

$$\gamma_{max}^{(N_1, N_2)} \approx \gamma_C \left(w_1^{(N_1)} + w_2^{(N_2)} \right) \qquad (17)$$

in which the subscripts 1 and 2 refer to the two surfaces in contact. For example, the adhesive force between two-hierarchical level surfaces, defined by $w_{1,2}^{(2)} = 1.75$ ($\varphi = 0.5, s=1$), is enhanced by hierarchy by a factor of 3.5 (with respect to the two corresponding flat surfaces). Note that for $s=10$ this factor becomes 18 and remains significantly larger than one (i.e. 10) even if one of the two surfaces becomes perfectly flat.

However we have to note that the Wenzel approach must loose its validity for large roughness w, for which an effective micro- (rather than macro-) roughness have to be considered.

Capillary and van der Waals Forces

The capillary force can also be derived according to the well-known Laplace's law [47]. The attractive force between two flat plates of areas A, separated by a liquid of thickness t, with (liquid/vapour) surface tension γ_C and (liquid/solid) contact angle θ is (see the review by [21]):

$$F_C = \frac{2A\gamma_C \cos \theta}{t} \qquad (18)$$

Note that $\sigma_C = F_C/A$ is a function of the liquid thickness but not of the size of the contact. Considering for example $\gamma_C = 0.05\,\text{N/m}$, $\theta = 80°$ and $t=1$ nm would yield $\sigma_C \approx 9$ MPa. The force described by Eq. 17 is attractive for $\theta < 90°$ (hydrophilic) or repulsive for $\theta > 90°$ (hydrophobic). An additional viscous force can be generated $F_C^{(\eta)} \propto \eta/\tau$, where η is the dynamic viscosity of the liquid and τ is the separation time interval.

Note the differences between the force predictions of Eq. 18 and that considered in the previous section [46], i.e.:

$$F_C = 2\pi r_0 \gamma_C \left(\cos\theta + \cos\theta_P\right) \qquad (19)$$

in the limit of $r_0 \to \infty$, which suggest that we are far from a full understanding of the mechanism. In addition, both the approaches predict $\sigma_C = F_C/A = F_C/(\pi r_0^2) \to \infty$ for $t, r_0 \to 0$ in contrast to the common sense of a finite theoretical strength $\sigma_C^{(th)}$. This cut-off could be a consequence of a quantized (instead of a continuous) crack propagation, as discussed in the example reported by Pugno [26]. Thus, the following asymptotic matching can be straightforwardly proposed:

$$\sigma_C \approx \left(\frac{2}{r_0 + c} + \frac{1}{t + c}\right) \gamma_C \left(\cos\theta + \cos\theta_P\right), c \approx 3\gamma_C \left(\cos\theta + \cos\theta_P\right) \Big/ \sigma_C^{(th)} \qquad (20)$$

Similarly, the van der Waals force between two parallel surfaces of area A is ([48]; see also [49]):

$$F_{vdW} = \frac{HA}{6\pi t^3} \qquad (21)$$

where H is the Hamaker's constant, with a typical value around 10^{-20} J (as before, $t<30$ nm is the separation between the two surfaces). Note that $\sigma_{vdW} = F_{vdW}/A$ is a function of the liquid thickness but not of the size of the contact. Considering for example $t=1$ nm would yield $\sigma_{vdW} \approx 0.5$ MPa.

For the case of a spherical surface of radius r_0 and a flat plate, the contact force predicted according to the 'JKR' model of contact mechanics [50] is:

$$F_{vdW} = 3/2\pi \gamma_{vdW} r_0 \qquad (22)$$

Thus also in this case, as formerly discussed by Arzt et al. [13], $F_n = \sqrt{n}F_1$. Moreover, since $F_{vdW} \propto r_0$ the results reported in the previous section are still applicable.

As for capillary, note the differences between the two approaches summarized in Eqs. 21 and 22, which suggest that we are far from a full understanding of the mechanism. In addition, Eqs. 21 and 22 predict $\sigma_{vdW} = F_{vdW}/A = F_{vdW}/(\pi r_0^2) \to \infty$

for $t, r_0 \to 0$ in contrast to the common sense of a finite theoretical strength $\sigma_{vdW}^{(th)}$ (and of a quantized crack propagation, see [26]). Thus, the following asymptotic matching can be straightforwardly proposed:

$$\sigma_{vdW} \approx 3/2\gamma_{vdW} \left(\frac{1}{r_0 + c} + \frac{H}{9\gamma_{vdW}\pi (t + c)^3} \right), c = X \left(6\pi \sigma_{vdW}^{(th)} ; -9\pi \gamma_{vdW} ; 0; -H \right)$$

(23)

where $X(a;b;c;d)$ denotes the solution of the three-order polynomial equation $ax^3 + bx^2 + cx + d = 0$, derived imposing c : $\sigma_{vdW}(r_0, t \to 0) = \sigma_{vdW}^{(th)}$ (one could also consider valid Eq. 23 with $c \to 0$, with a cut-off at $\sigma_{vdW}^{(th)}$). To have an idea of the theoretical strength note that $\sigma_{vdW}^{(th)} \approx 20$ MPa (see [51]).

The different force predictions for plausible values are of the same order of magnitude. Using Eq. 22, as done by Autumn et al. [4] and Arzt et al. [13], ($\gamma_{vdW} \approx 0.05$ N/m) for the gecko spatula ($r_0 \approx 0.05\,\mu$m) we get $F_{spatula} \approx 12$ nN, comparable to the observed value of ~ 11 nN [9]. Thus, for a seta composed by 1,000 spatulae, $F_{seta} \approx 12\,\mu$N [4, 8] measured values of ~ 194 and ~ 40 μN respectively); for a non hierarchical seta from Eq. 22 one would deduce ($r_0 \approx 5\,\mu$m) $F_{seta}' \approx 1.2\,\mu$N and thus for a real, thus hierarchical, seta having 1,000 spatulae, $F_{seta} \approx \sqrt{1000} \times 1.2\,\mu$N $\approx 38\,\mu$N. Similarly for the setula of a spider $R_{eq} \approx \sqrt{0.17/\pi}\,\mu$m $\approx 0.2\,\mu$m (terminal surface area of $\sim 0.17\,\mu$m^2) and $F_{setula} \approx 47$ nN (observed value ~ 41 nN, [5]).

Finally, we note that since different mechanisms could be simultaneously activated, the real adhesive force (or strength or fracture energy) could be computed as:

$$F = \sum_i F_i f_i$$

(24)

in which F_i is the force activated by the i-th mechanism having weight f_i $\left(\sum_i f_i = 1 \right)$.

For example, for geckos a still partially unsolved question is to quantify the participation of capillary and van der Waals forces in their adhesion (nanohook and suction mechanisms in geckos have been ruled out, see the review by [2]). We note that Huber et al. [3] observed a humidity (U) dependence of the adhesion force in gecko spatulae, thus, from Eq. 24 we could write:

$$F = F_{dry}f_{dry} + F_{wet}f_{wet} \approx F_{vdW} (1 - U) + (F_{vdW} + F_C) U$$

(25)

By fitting their data we find $F_{vdW} \approx 7$nN and $F_C \approx 5$nN, thus $F_{vdW}/F_C \approx 1.4$, i.e., van der Waals are expected to be the main adhesive forces in geckos even if capillary ones play a significant role too.

Equations 20 and 23 can be straightforwardly extended to hierarchical surfaces according to our findings reported in the previous Section.

Smart Adhesion

Consider the detachment as the peeling of a thin film of (free-) length l, width b and thickness h, pulled at an angle ϑ by a force F Fig. 7. A non-linear stress-strain relationship $\sigma = E(\varepsilon)\varepsilon$ is considered. The total potential energy (elastic energy minus external work) of the film is $\Phi = bhl \int_0^\varepsilon E(\varepsilon)\varepsilon \, d\varepsilon - Fl(1 - \cos\vartheta + \varepsilon)$. Thus, the energy release rate is:

$$2\Delta\gamma \equiv -\frac{1}{b}\frac{d\Phi}{dl} = -h\int_0^\varepsilon E(\varepsilon)\varepsilon \, d\varepsilon + \frac{F}{b}(1 - \cos\vartheta + \varepsilon) \qquad (26)$$

The detachment will take place when $\Delta\gamma \equiv \gamma \equiv \gamma_1 + \gamma_2 - \gamma_{12}$, where $\gamma_{1,2}$ are the surface energies of the two materials in contact and γ_{12} is that of the interface.

For quadratic nonlinearities, i.e., $E(\varepsilon) = E + E'\varepsilon$, a closed form solution is still reachable. Note that $E' < 0$ describes elastic-plastic materials (e.g., hooked surface with $\varphi > \varphi_C \approx \pi/39$, see [26]), whereas $E' > 0$ hyper-elastic ones (e.g., hooked surface with $\varphi < \varphi_C$). The detachment force is found in the following form:

$$\varepsilon_C = X\left(4E';\ 3E + 6E'(1 - \cos\vartheta)\ ;\ 6E(1 - \cos\vartheta)\ ;\ -12\gamma/h\right), F_C \qquad (27)$$
$$= AE(\varepsilon_C)\varepsilon_C$$

(as before $X(a;b;c;d)$ denotes the solution of the three-order polynomial equation $ax^3 + bx^2 + cx + d = 0$). For $E' \to 0$ the classical Kendall [52] prediction is recovered. Varying the pulling angle strong force variations are found, as can easily be evinced considering the simplest case in the limit of $E^{-1}, E' \to 0$, deducing $F_C = 2\gamma b/(1 - \cos\vartheta)$. Note that, also according to fracture mechanics, sub-contacts are safer ($b \to b/\sqrt{n}, F_n = \sqrt{n}F_1$; the paper by Pugno [26] shows that this cannot be ad infinitum).

Moreover the strongest attachment is achieved for $\vartheta = 0$ whereas the easier detachment for $\vartheta = \pi$. The ratio between the corresponding forces is:
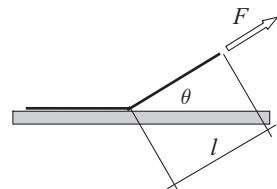

Fig. 7 Peeling of a thin film

$$\frac{F_a}{F_d} \equiv \frac{F_C\left(\vartheta = 0\right)}{F_C\left(\vartheta = \pi\right)} = g\left(E^{/}\right) \frac{1 + \sqrt{\chi + 1}}{\sqrt{\chi}}, \chi \equiv \gamma / (hE) \qquad (28)$$

where $g\left(E^{/}\right)$ is a known function describing the constitutive nonlinearity, which could have an important role for soft matter, and in particular $g\left(0\right) = 1$; in this case $F_a / F_d \rightarrow 1, \infty$ for $\chi \rightarrow \infty, 0$. For example taking $\gamma = 0.05 \mathrm{N}/\mathrm{m}$ (of the order of the previously discussed $\gamma_{h,C,vdW}$), $h = 100$ nm, $E = 10$ GPa we find $F_a / F_d \approx 283$. *This value is of the same order of magnitude of the safety factor found in spiders* [5], i.e., 173. Such a geometrical control can thus explain the smart safety factor reduction during detachment up to ~1, needed for animal walk. Thus, this pulling angle control can represent the main mechanism to achieve reversible adhesion. For example, for a man with adhesive gloves capable of supporting 300 kg at $\vartheta \approx \pi$, only ~1 kg must be applied at $\vartheta \approx 0$ to detach them. Probably the proper use of such hypothetical gloves would require opportune training, similarly to the use of a pair of skis, a paragliding or a wet suit.

The value of F_C corresponds to a delamination (opening and/or sliding) and not necessarily to a detachment (opening prevails on sliding). To distinguish between these two different mechanisms we note that $2\gamma = \left(K_{op}^2 + K_{sl}^2\right)/E$, where $K_{op,sl}$ are the stress intensity factors at the tip of the interfacial crack for opening (mode I) or sliding (mode II) and $K_{op} \propto F_\perp \propto \sin\vartheta$ whereas $K_{sl} \propto F_{//} \propto \cos\vartheta$; assuming as a first approximation a detachment for $K_{sl}/K_{op} \approx \tan^{-1}\vartheta < 1$ we derive a critical value of ~45°. A similar behaviour has recently been confirmed by numerical simulations on gecko seta [51]: for forces applied at an angle less than ~30° the predominant failure mode was sliding, whereas larger angles correspond to detachment. Using the previous parameters we find $F_C\left(\vartheta = 30°\right)/F_C\left(\vartheta = 150°\right) \approx 14$, which can still be sufficient to control adhesion of nonideal contacts, for which the strength is expected to be reduced by a factor of about one order of magnitude [12]. However note that in any case (i.e., also at $\vartheta \approx 0$) the total adhesive force could be overcome by subsequently detaching single points of contacts and not the whole surface at once [14], even if, when not in vivo, this mechanism could be hard to be activated. Note that the ratio predicted by Eq. 28 is compatible with homemade experiments that we have performed using adhesive tape. For larger thickness the behaviour would be that of a beam rather than of a film [26].

Observation on Living Geckos

In this section we summarize recent observations on adhesion of living geckos [53]. We report experimental observations on the times of adhesion of living Tokay geckos (*Gekko geckos*) on polymethylmethacrylate (PMMA) inverted surfaces. Two different geckos (male and female) and three surfaces with different root mean square (RMS) roughness (RMS=42, 618 and 931 nm) have been considered, for a total of 72 observations. The measured data are proved to be statistically significant, following the Weibull Statistics with coefficients of correlation between

0.781 and 0.955. The unexpected result is the observation of a maximal gecko adhesion on the surface with intermediate roughness of RMS=618 nm, that we note has waviness comparable to the seta size.

Surface roughness strongly influences the animal adhesion strength and ability. Its role was shown in different measurements on flies and beetles, walking on surfaces with well defined roughness [54], [55, 56], on the chrysomelid beetle *Gastrophysa viridula* [57], on the fly *Musca domestica* ([56]) as well as on the Tokay geckos [58]. Peressadko and Gorb [56] and Gorb [57] report a minimum of the adhesive/frictional force, spanning surface roughness from 0.3 to 3 µm. The experiments on the reptile Tokay gecko [58] showed a minimum in the adhesive force of a single spatula at an intermediate root mean square (RMS) surface roughness around 100–300 nm, and a monotonic increase of adhesion times of living geckos by increasing the RMS, from 90 to 3,000 nm. There are several observations and models in the literature, starting with the pioneer paper by Fuller and Tabor [59], in which roughness was seen to decrease adhesion monotonically. But there is also experimental evidence in the literature, starting with the pioneer paper by Briggs and Briscoe [60], which suggests that roughness need not always reduce adhesion. For example, Persson and Tosatti [61] and Persson [62], in the framework of a reversible model, have shown that for certain ranges of roughness parameters, it is possible for the effective surface energy to first increase with roughness amplitude and then eventually decreasing. Including irreversible processes, due to mechanical instabilities, Guduru [63] has demonstrated, under certain hypotheses, that the pull-out force must increase by increasing the surface wave amplitude. We have suggested [53] that roughness alone could not be sufficient to describe the three-dimensional topology of a complex surface and additional parameters have to be considered for formulating a well-posed problem.

Accordingly, we have machined and characterized three different Polymethylmethacrylate surfaces (PMMA 1,2,3; surface energy of ∼41 mN/m) with a full set of roughness parameters, as reported in Table 1: Sa represents the surface arithmetical average roughness; Sq=RMS is the classical mean square roughness; Sp and Sv are respectively the height of the highest peak and the deepness of the deepest valley (absolute value); Sz is the average distance between the five highest peaks and the five deepest valleys (detected in the analyzed area);

Table 1 Roughness parameters for the three different Polymethylmethacrylate (PMMA 1,2,3) surfaces

	PMMA1	PMMA2	PMMA3
Sa(µm)	0.033±0.0034	0.481±0.0216	0.731±0.0365
Sq(µm)	0.042±0.0038	0.618±0.0180	0.934±0.0382
Sp(µm)	0.252±0.0562	2.993±0.1845	4.620±0.8550
Sv(µm)	0.277±0.1055	2.837±0.5105	3.753±0.5445
Ssk	−0.122±0.1103	0.171±0.1217	0.192±0.1511
Sz (µm)	0.432±0.1082	4.847±0.2223	6.977±0.2294
Sdr (%)	0.490±0.0214	15.100±1.6093	28.367±2.2546

Ssk indicates the surface skewness; Sdr is the effective surface area minus the nominal one and divided by the last one.

   Two different Tokay gecko's, female (G1, weight of ~46 g) and male (G2, weight of ~72 g), have been considered. The gecko is first placed in its natural position on the horizontal bottom of a box ($50 \times 50 \times 50$ cm^3). Then, slowly, we rotated the box up to the gecko reaches a natural downwards position and, at that time, we start the measurement of the gecko time of adhesion. We excluded any trial in which the gecko walks on the inverted surface. The time measurement was stopped when gecko breaks loose from the inverted surface and falls on the bottom of the box (for G1) or at the first detachment movement of the gecko's foot (for G2). The time between one measurement and the following, pertaining to the same set, is only that needed to rotate the box and placed the gecko again on the upper inverted surface (~14 s). The experiments were performed at ambient temperature (~22°C) and humidity (~75%). The measured adhesion times are summarized in Table 2 and confirmed to be statistically significant by applying Weibull Statistics, see Fig. 8.

Table 2   Gecko adhesion times on PMMA 1,2,3 surfaces

Test No.	PMMA 1	PMMA 2	PMMA 3
1	8	137	15
2	13	215	22
3	36	243	22
4	37	280	25
5	48	498	27
6	62	610	29
7	67	699	32
8	87	900	35
9	88	945	48
10	93	1,194	51
11	116	1,239	53
12	134	1,320	91
13	145	2,275	97
14	160	2,740	102
15	197	4,800	109
16	212		114
17	215		148
18	221		207
19	228		424
20	292		645
21	323		
22	369		
23	474		
24	550		
25	568		
26	642		
27	660		
28	700		
29	707		
30	936		

Table 2 (continued)

Test No.	PMMA 1	PMMA 2	PMMA 3
31	1,268		
32	1,412		
33	1,648		
34	1,699		
35	2,123		
36	2,703		
37	2,899		
Scale Parameter t_0 (s)	800	1,251.7	108.4
Sq (μm)	0.042±0.0038	0.618±0.0180	0.934±0.0382

Note that, as an index of the gecko adhesion ability, here we use the Weibull scale parameter t_0 (in seconds) of the distribution of the detachment/failure F (closely related to its mean value)
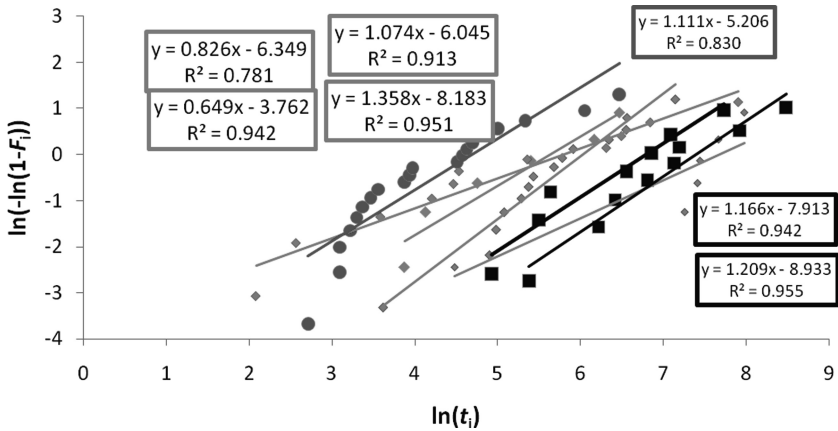

Fig. 8 Weibull Statistics (F is the cumulative probability of detachment/failure and t_i are the measured adhesion times) applied to the measured adesion times on PMMA surfaces. PMMA 1 (green, for which we made the measurements in four different days and with both geckos G1 and G2), PMMA 2 (black, for which we made the measurements in two different days, one with gecko G1 and one with gecko G2) and PMMA 3 (red, for which we made the measurements in a single day with gecko G2)

We have observed a maximum in the gecko's adhesion times on PMMA 2, having an intermediate roughness of RMS=618 nm. An oversimplified explanation could be the following. For PMMA 1 (Sq=42 nm, waviness of λ≈3–4 μm, h≈0.1 μm), the gecko's seta (diameter of ~10 μm, represented in blue in Fig. 9, that must not be confused with the terminal nearly two dimensional spatualae) cannot penetrate in the characteristic smaller valleys and adhere on the side of each single one Fig. 9a, thus cannot optimally adapt to the surface roughness. For PMMA 2 (Sq=618 nm, λ≈7–8 μm, h≈1 μm) the gecko's setae are able to adapt better to the roughness, adhering this time on the top of and on the side of a single asperity: in this way the effective number of setae in contact increases and, as a direct consequence, also
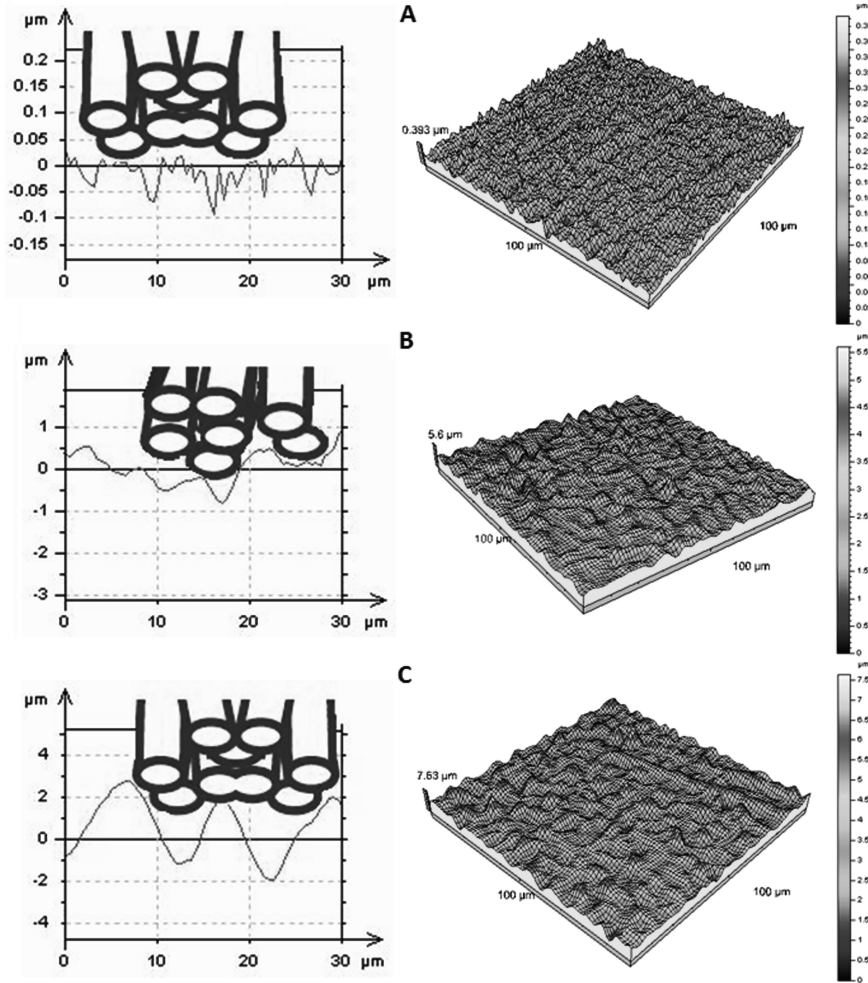
Fig. 9 A simple interpretation of our experimental results on the adhesion tests of living geckos on PMMA surfaces having different roughness. (**A**) Setae cannot adapt well on PMMA 1; (**B**) on PMMA 2 the adhesion is enhanced thanks to the higher compatibility in size between setae and roughness; (**C**) on PMMA 3 only partial contact is achieved. On the right, we report the analyzed three-dimensional profiles of the roughness for all the three investigated surfaces (from the top: PMMA 1,2 and 3)

the adhesion ability of the gecko increases Fig. 9b. On PMMA 3 ($Sq=931$ nm, $\lambda \approx 10$–12 µm and $h \approx 2$ µm) the waviness characterizing the roughness is larger than the seta's size: as a consequence, a decrease in the number of setae in contact is expected Fig. 9c . As a result, on PMMA 2 an adhesion increment, of about 45%, is observed. According to Briggs and Briscoe [60] an increment of 40%, thus close to our observation, is expected for an adhesion parameter α equal to 1/3. Such a

parameter was introduced as the key parameter in governing adhesion by Fuller and Tabor [59] as:

$$\alpha = \frac{4\sigma}{3} \left(\frac{4E}{3\pi \sqrt{\beta}\gamma} \right)^{2/3} \tag{29}$$

where σ is the standard deviation of the asperity height distribution (assumed to be Gaussian), β is the mean radius of curvature of the asperity, γ is the surface energy and E is the Young modulus of the soft solid (gecko foot). Even if the value of E of the entire foot cannot be simply defined, as a consequence of its non compact structure, we note that considering it to be of the order of 10 MPa (thus much smaller than that of the keratin material), with $\gamma \approx 0.05 \,\text{N/m}$ [8], $\sigma \approx$ Sq, $\beta \approx \lambda$ would correspond to values of α close to 0.5.

The reported maximal adhesion was not observed by Huber et al. [58]. Note that their tested polished surfaces were of five different types, with a nominal asperity size of 0.3, 1, 3, 9 and 12 µm, which correspond to RMS values of 90, 238, 1,157, 2,454 and 3,060 nm respectively. Huber et al. [58] have observed sliding of geckos on polishing paper with a RMS value of 90 nm for slopes larger than 135°. On a rougher substrate, with a RMS value of 238 nm, two individual geckos were able to cling to the ceiling for a while, but the foot-surface contact had to be continuously renewed because gecko toes slowly tend to slid off the substrate. Finally, on the remaining tested rougher substrates, animals were able to adhere stably to the ceiling for more than 5 min.

These different observations (assuming that the influences of claws and moult were minimized also by Huber et al. [58] suggest that the RMS parameter is not sufficient alone to describe all the aspects of the surface roughness. The use of a 'complete'set of roughness parameters could help in better understanding the animal adhesion and thus in optimizing the Spiderman suit design.

Towards a Spiderman Suit

According to our analysis, a man (palm surfaces of $\sim$200 cm^2) and gecko-material gloves ($\sigma_{gecko} \approx 0.58$ MPa) could support a mass of $\sim$1,160 kg (safety factor $\sim$14), or with spider-material gloves ($\sigma_{spider} \approx 0.24$ MPa) a mass of $\sim$480 kg (safety factor $\sim$6). We expect, due to non ideal contact, a safety factor reduction of about one order of magnitude [12], thus we still conclude that Spiderman suits could become feasible in the near future. Note that theoretical van der Waals gloves ($\sigma_{vdW}^{(th)} \approx 20$ MPa) would allow one to support a mass of $\sim$40,000 kg (safety factor of $\sim$500). Carbon nanotubes could be one of the most promising candidates for our applications: on a small scale a carbon nanotube surface was able to achieve adhesive forces $\sim$200 times greater than those of gecko foot hairs [64], even if it could not replicate large scale gecko adhesion perhaps due to a lack of compliance and hierarchy. Thus, we propose the use of hierarchical branched long (to have the

sufficient compliance) nanotubes [65] as good material for a Spiderman suit, with a number of hierarchical levels sufficient to activate self-cleaning, as quantifiable by our calculations. Their aspect ratio must not be too large, to avoid bunching [66, 67] and elastic self-collapse under their own weight, but sufficiently large to conform to a rough surface by buckling under the applied stress (see [2]), similar to the optimization done by Nature in spiders and geckos. In particular, following Glassmaker et al. [67] and Yao and Gao [68] for the bunching and introducing our result for the pillar radius at the level N ($r_N = r_0 \left(\varphi/n \right)^{N/2}$) we find the anti-bunching and anti-self-collapse [69] conditions at the hierarchical level N in the following form:

$$s < \min \left\{ 2 \left(\frac{3^3 \pi^4}{2^5 \left(1 - v^2 \right)} \right)^{1/12} \left(\frac{Er_0}{\gamma} \right)^{1/3} \left(\frac{\varphi}{n} \right)^{N/6} \left(\sqrt{\left(\varphi_{max}/\varphi^N \right)} - 1 \right)^{1/2}, \right.$$

$$\left. \left(\frac{8\pi^2 E}{r_0 \left(\varphi/n \right)^{N/2} \rho g} \right)^{1/3} \right\},$$

$$(29)$$

where v is the Poisson's ratio, ρ is the material density and $\varphi_{max} = \pi \big/ 2\sqrt{3}$, $\varphi_{max} = \pi \big/ 4$ or $\varphi_{max} = \pi \big/ 3\sqrt{3}$ for triangular, square or hexagonal pillar lattices respectively. In order to have a uniform contact, the buckling [69] must be activated under the applied stress σ_a (e.g., ~10 KPa, see [2]), thus imposing:

$$s > \pi \sqrt{4/3} \varphi^{N/2} \sqrt{\left(\sigma_a/E \right)}, \tag{30}$$

Equations 29 and 30 can be used for an optimal design of hierarchical super-adhesive materials.

Accompanied by large transparent (if not fully invisible, to dispose of a higher strength) nanotube based cobwebs, a complete preliminary Spiderman suit could be realized, Fig. 2.

Conclusions

We have proposed [26] new laws to design futuristic self-cleaning, super-adhesive and releasable hierarchical smart materials, as well as large invisible cables, based on carbon nanotube technology.

Thus the formulas suggest the possibility of scaling up the amazing adhesion properties of a spider to the size of a man, thus the feasibility of a Spiderman suit. Strong attachment and self-cleaning are all properties that must be achieved simultaneously. Even if this seems to be impossible, since these mechanisms are in strong competitions, lotus leaves and gecko feet suggest the opposite. But one could deduce that this high nanotech project is unfeasible, since no adhesive-based animals larger than geckos exist in Nature. This is not fully right: Nature has often different scopes

with respect to ours, for example animals are not interested in going into space, as we are. Consequently, rather than mimicking Nature we must be inspired by Nature: an airplane is not a big bird. Thus, the project could be feasible. We think that it is feasible, since for a Spiderman Suit we need an adhesive strength that is much lower (two order of magnitudes) than the theoretical (e.g. van der Waals) strength. This safety factor could allow us to produce a flaw-tolerant, a very important requirement since larger contact imperfections are expected at larger size scales, super-adhesive smart material.

The analysis thus represents a first step towards the feasibility of a Spiderman suit [26].

References

1. B. Bhushan, J.N. Israelachvili, U. Landman, Nanotribology: friction, wear and lubrication at the atomic scale. Nature **374**, 607–616 (1995)
2. B. Bhushan, A. Sayer, *Gecko Feet: Natural Attachment Systems for Smart Adhesion*, Applied Scanning Probe Methods – Biomimetics and Industrial Applications, vol 7 (Springer-Verlag, Heidelberg, Germany, 2007), p. 41–76
3. G. Huber, H. Mantz, R. Spolenak, K. Mecke, K. Jacobs, S.N. Gorb, E. Arzt, Evidence for capillarity contributions to gecko adhesion from single spatula and nanomechanical measurements. Proc. Natl. Acad. Sci. U.S.A. **102**, 16293–16296 (2005a)
4. K. Autumn, M. Sitti, Y.A. Liang, A.M. Peattie, W.R. Hansen, S. Sponberg, T.W. Kenny, R. Fearing, J.N. Israelachvili, R.J. Full, Evidence for van der Waals adhesion in gecko setae. Proc. Natl. Acad. Sci. U.S.A. **99**, 12252–12256 (2002)
5. A.B. Kesel, A. Martin, T. Seidl, Getting a grip on spider attachment: an AFM approach to microstructure adhesion in arthropods. Smart Mater. Struct. **13**, 512–518 (2004)
6. R. Ruibal, V. Ernst, The structure of the digital setae of lizards. J. Morph. **117**, 271–294 (1965)
7. H.H. Schleich, W. Kästle, Ultrastrukturen an Gecko-Zehen. Amphib. Reptil. **7**, 141–166 (1986)
8. K. Autumn, Y.A. Liang, S.T. Hsieh, W. Zesch, W.P. Chan, T.W. Kenny, R. Fearing, R.J. Full, Adhesive force of a single gecko foot-hair. Nature **405**, 681–685 (2000)
9. G. Huber, S.N. Gorb, R. Spolenak, E. Arzt, Resolving the nanoscale adhesion of individual gecko spatulae by atomic force microscopy. Biol. Lett. **1**, 2–4 (2005b)
10. W. Federle, K. Rohrseitz, B. Hölldobler, Attachment forces of ants measured with a centrifuge: better 'wax-runners' have a poorer attachment to a smooth surface. J. Exp. Biol. **203**, 505–12 (2000)
11. N.E. Stork, Experimental analysis of adhesion of *Chrysolina polita* (Chrysomelidae: Coleoptera) on a variety of surfaces. J. Exp. Biol. **88**, 91–107 (1983)
12. N. Pugno, On the strength of the nanotube-based space elevator cable: from nanomechanics to megamechanics. J. Phys. Condens. Matter **18**, S1971–S1990 (2006a)
13. E. Arzt, S. Gorb, R. Spolenak, From micro to nano contacts in biological attachment devices. Proc. Natl. Acad. Sci. U.S.A. **100**, 10603–10606 (2003)
14. S. Niederegger, S. Gorb, Tarsal movements in flies during leg attachment and detachment on a smooth substrate. J. Insect Physiol. **49**, 611–20 (2003)
15. M. Varenberg, N. Pugno, S. Gorb, Spatulae structures in biological fibrillar adhesion. SOFT MATTER **6**, 3269–3272 (2010)
16. C. Neinhuis, W. Barthlott, Characterisation and distribution of water-repellent, self-cleaning plant surfaces. Ann. Bot. **79**, 667–677 (1997)

17. W. Barthlott, C. Neinhuis, Purity of scared lotus or escape from contamination in biological surfaces. Planta **202**, S1–8 (1997)
18. T. Wagner, C. Neinhuis, W. Barthlott, Wettability and contaminability of insect wings as a function of their surface sculture. Acta Zool. **77**, 213–225 (1996)
19. W. Lee, M.K. Jin, W.C. Yoo, J.K. Lee, Nanostructuring of a polymeric substrate with well- defined nanometer-scale topography and tailored surface wettability. Langmuir **20**, 7665–7669 (2004)
20. X. Gao, L. Jiang, Biophysics: water-repellent legs of water striders. Nature **432**, 36 (2004)
21. D. Quéré, Non-sticking drops. Rep. Prog. Phys. **68**, 2495–2532 (2005)
22. R. Blossey, Self-cleaning surfaces – virtual realities. Nat. Mater. **2**, 301–306 (2003)
23. W.R. Hansen, K. Autumn, Evidence for self-cleaning in gecko setae. Proc. Natl. Acad. Sci. U.S.A. **102**, 385–389 (2005)
24. A.K. Geim, S.V. Dubonos, I.V. Grigorieva, K.S. Novoselov, A.A. Zhukov, S.Y. Shapoval, Microfabricated adhesive mimicking gecko foot-hair. Nat. Mater. **2**, 461–463 (2003)
25. N. Pugno, Large invisible cables Arxiv: cond-mat/0601369 (2006b)
26. N. Pugno, Towards a Spiderman suit: large invisible cables and self-cleaning releasable super-adhesive materials. J. Phys. Condens. Mater **19**, 395001–395018 (2007a)
27. N. Pugno, Spiderman gloves. Nano Today **3**, 35–41 (2008)
28. M. Zhang, S. Fang, A.A. Zakhidov, S.B. Lee, A.E. Aliev, C.D. Williams, K.R. Atkinson, R.H., Strong, transparent, multifunctional, carbon nanotube sheets. Science **309**, 1215–1219 (2005)
29. M.F. Yu, O. Lourie, M.J. Dyer, K. Moloni, T.F. Kelly, R.S. Ruoff, Strength and breaking mechanism of multiwalled carbon nanotubes under tensile load. Science **287**, 637–640 (2000)
30. A. Carpinteri, N. Pugno, Are the scaling laws on strength of solids related to mechanics of to geometry? Nat. Mater. **4**, 421–423 (2005)
31. N. Pugno, Graded cross-links for stronger nanomaterials. Mater. Today **13**, 40–43 (2010)
32. N. Pugno, Velcro® nonlinear mechanics. Appl. Phys. Lett. **90**, 121918 (2007b)
33. A. Carpinteri, *Structural Mechanics: A Unified Approach* (E & FN Spon, London, UK, 1997)
34. D. Kretschmann, Velcro mechanics in wood. Nat. Mater. **2**, 775–776 (2003)
35. A.P. Russell, The morphological basis of weight-bearing in the scansors of the tokay gecko. Can. J. Zool. **64**, 948–955 (1986)
36. J.E.A. Bertram, J.M. Gosline, Functional design of horse hoof keratin: the modulation of mechanical properties through hydration effects. J. Exp. Biol. **130**, 121–136 (1987)
37. K. Autumn, A.M. Mechanisms of adhesion in geckos. Integr. Comp. Biol. **42**, 1081–1090 (2002)
38. T. Young, An essay on the cohesion of fluids. Phil. Trans. R. Soc. (London) **95**, 65–87 (1805)
39. R.N. Wenzel, Resistance of solid surfaces to wetting by water. Ind. Eng. Chem. **28**, 988–994 (1936)
40. R.N. Wenzel, Surface roughness and contact angle. J. Phys. Chem. **53**, 1466–70 (1949)
41. A.B.D. Cassie, S. Baxter, Wettability of porous surfaces. Trans. Faraday Soc. **40**, 546–551 (1944)
42. D. Quéré, Fakir droplets. Nat. Mater. **1**, 14–15 (2002)
43. J. Bico, U. Thiele, D. Quèrè, Wetting of textured surfaces. Colloids Surf. A **206**, 41–46 (2002)
44. J. Bico, C. Marzolin, D. Quèrè, Pearl drops. Europhys. Lett. **47**, 220–226 (1999)
45. T. Eisner, D.J. Aneshansley, Defense by foot adhesion in a beetle (Hemisphaerota cyanea). Proc. Natl Acad. Sci. U.S.A. **97**, 6568–6573 (2000)
46. J.S. McFarlane, D. Tabor, Adhesion of solids and the effects of surface films. Proc. R. Soc. (London) A **202**, 224–243 (1950)
47. P.S. Laplace, *Oeuvres Complètes* (Imprimerie Royale, Paris, 1847)
48. H.C Hamaker, The London-van der Waals attraction between spherical particles. Physica **4**, 1058–1072 (1937)
49. J.N. Israelachvili, *Intermulecular and Surface Forces, with Application to Colloidal and Biological Systems* (Colloid Science S.) (Academic Press Inc., San Diego, CA, 1991)
50. K.L. Johnson, K. Kendall, A.D. Roberts, Surface energy and the contact of elastic solids. Proc. R. Soc. (London) A **324**, 301–313 (1971)

51. H. Gao, X. Wang, H. Yao, S. Gorb, E. Arzt, Mechanics of hierarchical adhesion structures of geckos. Mech. Mater. **37**, 275–285 (2005)
52. K. Kendall, Thin-film peeling-elastic term. J. Phys. D: Appl. Phys. **8**, 1449–1452 (1975)
53. N. Pugno, E. Lepore, Observation of optimal gecko's adhesion on nanorough surfaces. Biosystems **94**, 218–222 (2008)
54. Z. Dai, S.N. Gorb, U. Schwarz, Roughness-dependent friction force of the tarsal claw system in the beetle Pachnoda marginata (Coleoptera Scarabaeidae). J. Exp. Biol. **205**, 2479–2485 (2002)
55. B.N.J. Persson, S. Gorb, The effect of surface roughness on the adhesion of elastic plates with application to biological systems. J. Chem. Phys. **119**, 11437–11444 (2003)
56. A.G. Peressadko, S.N. Gorb, *Surface Profile and Friction Force Generated by Insects*, vol 15, ed. by I. Boblan, R. Bannasch (Bionik, Hannover; 2004) p. 237
57. S.N. Gorb, *Attachment Devices of Icuticle* (Dordrecht: Kluwer Academic Publishers, Boston, 2001)
58. G. Huber, S.N. Gorb, N. Hosoda, R. Spolenak, E. Arzt, Influence of surface roughness on gecko adhesion. Acta Biomater. **3**, 607–610 (2007)
59. K.N.G. Fuller, D. Tabor, The effect of surface roughness on the adhesion of elastic solids. Proc. Royal Soc. Lond. A **345**, 327–342 (1975)
60. G.A.D. Briggs, B.J. Briscoe, The effect of surface topography on the adhesion of elastic solids. J. Phys. D: Appl. Phys. **10**, 2453–2466 (1977)
61. B.N.J. Persson, E. Tosatti, The effect of surface roughness on the adhesion of elastic solids. J. Chem. Phys. **115**, 5597–5610 (2001)
62. B.N.J. Persson, Adhesion between and elastic body and a randomly hard surface. Eur. Phys. J. E **8**, 385–401 (2002)
63. P.R. Guduru, Detachment of a rigid solid from an elastic wavy surface: theory. J. Mech. Phys. Solids **55**, 445–472 (2007)
64. B. Yurdumakan, N.R. Raravikar, P.M. Ajayan, A. Dhinojwala, Synthetic gecko foot hairs from multiwalled carbon nanotubes. Chem. Comm. **30**, 3799–3801 (2005)
65. G. Meng, Y.J. Jung, A. Cao, R. Vajtai, P.M. Ajayan, Controlled fabrication of hierarchically branched nanopores, nanotubes, and nanowires. Proc. Natl. Acad. Sci. U.S.A. **102**, 7074–7078 (2005)
66. C.Y. Hui, A. Jagota, Y.Y, Lin, E.J. Kramer, Constraints on micro-contact printing imposed by stamp deformation. Langmuir **18**, 1394–1404 (2002)
67. N.J. Glassmaker, A. Jagota, C.Y. Hui, J. Kim, Design of biomimetic fibrillar interface: 1. Making contact. J. R. Soc. Interface London **1**, 23–33 (2004)
68. H. Yao, H. Gao, Mechanics of robust and releasable adhesion in biology: bottom-up designed of hierarchical structures of gecko. J. Mech. Phys. Sol. **54**, 1120–1146 (2006)
69. S.P. Timoshenko, J.M. Gere, *Theory of Elastic Stability* (McGraw-Hill, New York, 1961)
70. U. Hiller, Untersuchungen zum Feinbau und zur Funktion der Haftborsten von Reptilien. Z Morphol Tiere **62**, 307–362 (1968)
71. A.P. Russell, A contribution to the functional morphology of the foot of the tokay, Gekko gecko. J. Zool. Lond. **176**, 437–476 (1975)
72. E.E. Williams, J.A. Peterson, Convergent and alternative designs in the digital adhesive pads of scincid lizards. Science **215**, 1509–1511 (1982)
73. W. Sun, P. Neuzil, T.S. Kustandi, S. Oh, V.D. Samper, The nature of the gecko Lizard Adhesive Force. Biophys. J. **89**, L14–L17 (2005)
74. A.B. Kesel, A. Martin, T. Seidl, Adhesion measurements on the attachment devices of the jumping spider Evarcha arcuata. J. Exp. Biol. **206**, 2733–2738 (2003)
75. K.K.S. Lau, J. Bico, K.B.K. Teo, M. Chhowalla, G.A.J. Amaratunga, W.I. Milne, G.H. McKinley, K.K., Superhydrophobic carbon nanotube forests. Nanoletters **3**, 1701–1705 (2003)
76. N. Pugno, R. Ruoff, Quantized fracture mechancis. Phil. Mag. **84**, 2829–2845 (2004)

Strength of Nanotubes and Megacables

Nicola M. Pugno

Abstract In this chapter my findings [mainly reported in N. Pugno, J. Phys.–Condens. Matter, **18**, S1971–S1990 (2006); N. Pugno, Acta Mater. **55**, 5269–5279 (2007); N. Pugno, Nano Today **2**, 44–47 (2007)] on the mechanical strength of nanotubes and megacables are reviewed, with an eye to the challenging project of the carbon nanotube-based space elevator megacable. Accordingly, basing the design of the megacable on the theoretical strength of a single carbon nanotube, as originally proposed at the beginning of the third millennium, has been demonstrated to be naïve. The role on the fracture strength of thermodynamically unavoidable atomistic defects with different size and shape is thus here quantified on brittle fracture both numerically (with *ad hoc* hierarchical simulations) and theoretically (with quantized fracture theories), for nanotubes and nanotube bundles. Fatigue, elasticity, non-asymptotic regimes, elastic-plasticity, rough cracks, finite domains and size-effects are also discussed.

Introduction

A space elevator basically consists of a cable attached to the Earth surface for carrying payloads into space [1]. If the cable is long enough, i.e. around 150 Mm (a value that can be reduced by a counterweight), the centrifugal forces exceed the gravity of the cable, that will work under tension [2]. The elevator would stay fixed geosynchronously; once sent far enough, climbers would be accelerated by the Earth's rotational energy. A space elevator would revolutionize the methodology for carrying payloads into space at low cost, but its design is very challenging. The most critical component in the space elevator design is undoubtedly the cable [3–5], that requires a material with very high strength and low density.

N.M. Pugno (✉)
Department of Structural Engineering and Geotechnics, Politecnico di Torino,
Corso Duca degli Abruzzi 24, 10129 Torino, Italy
e-mail: nicola.pugno@polito.it

Considering a cable with constant cross-section and a vanishing tension at the planet surface, the maximum stress-density ratio, reached at the geosynchronous orbit, is for the Earth equal to 63 GPa/(1,300 kg/m^3), corresponding to 63 GPa if the low carbon density is assumed for the cable. Only recently, after the re-discovery of carbon nanotubes [6], such a large failure stress has been experimentally measured, during tensile tests of ropes composed of single walled carbon nanotubes [7] or multiwalled carbon nanotubes [8] both expected to have an ideal strength of ~100 GPa. Note that for steel (density of 7,900 kg/m^3, maximum strength of 5 GPa) the maximum stress expected in the cable would be of 383 GPa, whereas for kevlar (density of 1,440 kg/m^3, strength of 3.6 GPa) of 70 GPa, both much higher than their strengths [3].

However, an optimized cable design must consider a uniform tensile stress profile rather than a constant cross-section area [2]. Accordingly, the cable could be built of any material by simply using a large enough taper-ratio, that is the ratio between the maximum (at the geosynchronous orbit) and minimum (at the Earth's surface) cross-section area. For example, for steel or kevlar a giant and unrealistic taper-ratio would be required, 10^{33} or 2.6×10^8 respectively, whereas for carbon nanotubes it must theoretically be only 1.9^9. Thus, the feasibility of the space elevator seems to become only currently plausible [9, 10] thanks to the discovery of carbon nanotubes. The cable would represent the largest engineering structure, hierarchically designed from the nano- (single nanotube with length of the order of a hundred nanometers) to the mega-scale (space elevator cable with a length of the order of a hundred megameters).

In this chapter the asymptotic analysis on the role of defects for the mega-cable strength, based on new theoretical deterministic and statistical approaches of quantized fracture mechanics proposed by the author [11–14], is extended to non asymptotic regimes, elastic-plasticity, rough cracks and finite domains. The role of thermodynamically unavoidable atomistic defects with different size and shape is thus quantified on brittle fracture, fatigue and elasticity, for nanotubes and nanotube bundles. The results are compared with atomistic and continuum simulations and nano-tensile tests of carbon nanotubes. Key simple formulas for the design of a flaw-tolerant space elevator megacable are reported, suggesting that it would need a taper-ratio (for uniform stress) of about two orders of magnitude larger than as today erroneously proposed.

The chapter is organized in 10 short sections, as follows. After this introduction, reported as the first section, we start calculating the strength of nanotube bundles by using *ad hoc* hierarchical simulations, discussing the related size-effect. In Sect. 'Brittle Fracture' the strength reduction of a single nanotube and of a nanotube bundle containing defects with given size and shape is calculated; the taper-ratio for a flaw-tolerant space elevator cable is accordingly derived. In Sect. 'Elastic-Plasticity, Fractal Cracks and Finite Domains' elastic-plastic (or hyper-elastic) materials, rough cracks and finite domains are discussed. In Sect. 'Fatigue' the fatigue life time is evaluated for a single nanotube and for a nanotube bundle. In Sect. 'Elasticity' the related Young's modulus degradations are quantified. In Sects. 'Atomistic Simulations', 'Nanotensile Tests' we compare our results on strength

and elasticity with atomistic simulations and tensile tests of carbon nanotubes. In Sect. 'Thermodynamic Limit' we demonstrate that defects are thermodynamically unavoidable, evaluating the minimum defect size and corresponding maximum achievable strength. The last section presents our concluding remarks.

Hierarchical Simulations and Size-Effects

To evaluate the strength of carbon nanotube cables, the SE[3] algorithm, formerly proposed [3] has been adopted [15]. Multiscale simulations are necessary in order to tackle the size scales involved, spanning over $\sim$10 orders of magnitude from nanotube length ($\sim$100 nm) to kilometre-long cables, and also to provide useful information about cable scaling properties with length.

The cable is modelled as an ensemble of stochastic 'springs', arranged in parallel sections. Linearly increasing strains are applied to the fibre bundle, and at each algorithm iteration the number of fractured springs is computed (fracture occurs when local stress exceeds the nanotube failure strength) and the strain is uniformly redistributed among the remaining intact springs in each section.

In-silico stress-strain experiments have been carried out according to the following hierarchical architecture. Level 1: the nanotubes (single springs, Level 0) are considered with a given elastic modulus and failure strength distribution and composing a $40\times1{,}000$ lattice or fibre. Level 2: again a $40\times1{,}000$ lattice composed by second level 'springs', each of them identical to the entire fibre analysed at the first level, is analysed with in input the elastic modulus and stochastic strength distribution derived as the output of the numerous simulations to be carried out at the first level. And so on. Five hierarchical levels are sufficient to reach the size-scale of the megametre from that of the nanometre, Fig. 1.

The level 1 simulation is carried out with springs $L_0 = 10^{-7}$ m in length, $w_0 = 10^{-9}$ m in width, with Young's modulus $E_0 = 10^{12}$ Pa and strength σ_f randomly distributed according to the nanoscale Weibull statistics [16] $P(\sigma_f) = 1 - \exp[-(\sigma_f/\sigma_0)^m]$, where P is the cumulative probability. Fitting to experiments [7, 8], we have derived for carbon nanotubes $\sigma_0 = 34$ GPa and $m = 2.7$ [16]. Then the level 2 is computed, and so on. The results are summarized in Fig. 2, in which a strong size-effect is observed, up to length of $\sim$1 m.

Given the decaying σ_f vs. cable length L obtained from simulations, it is interesting to fit the behaviour with simple analytical scaling laws. Various exist in the literature, and one of the most used is the Multi-Fractal Scaling Law (MFSL [17], see also [18]) proposed by Carpinteri. This law has been recently extended towards the nanoscale [19]:

$$\frac{\sigma_f}{\sigma_{macro}} = \sqrt{1 + \frac{l_{ch}}{L + l_0}} \tag{1}$$

where σ_f is the failure stress, σ_{macro} is the macrostrength, L is the structural characteristic size, l_{ch} is a characteristic internal length and l_0 is defined via
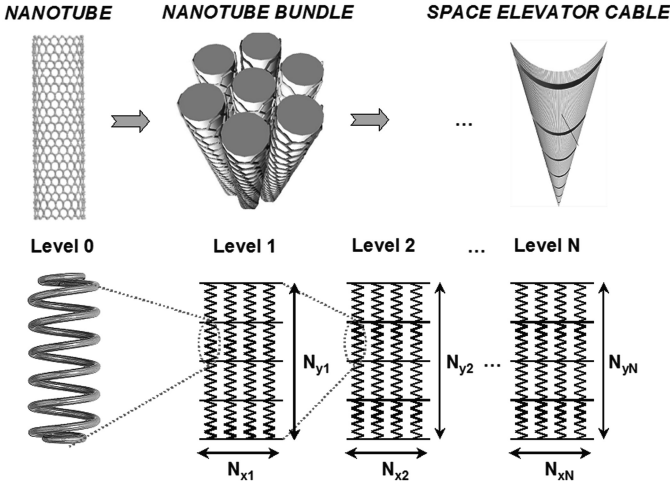
Fig. 1 Schematization of the adopted multiscale simulation procedure to determine the space elevator cable strength. Here, $N = 5$, $N_{x1} = N_{x2} = \ldots N_{x5} = 40$ and $N_{y1} = N_{y2} = \ldots N_{y5} = 1,000$, so that the total number of nanotubes in the space elevator cable is $N_{tot} = (1,000 \times 40)^5 \approx 10^{23}$ [15]
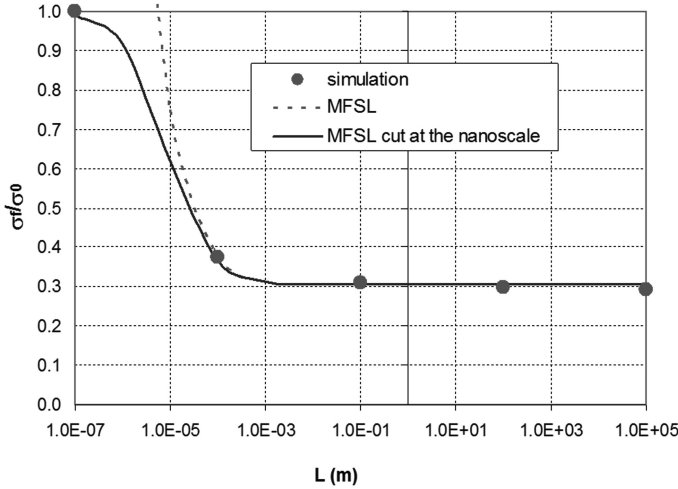

Fig. 2 Comparison between simulations and analytical scaling law Eq. 1 for the failure strength of the nanotube bundle as a function of its length; the asymptote is at 10.20 GPa [15]

$\sigma_f (l = 0) = \sigma_{macro}\sqrt{1 + \frac{l_{ch}}{l_0}} \equiv \sigma_{nano}$, where σ_{nano} is the nanostrength. Note that for $l_0 = 0$ this law is identical to the Carpinteri' scaling law [17]. Here, we can choose σ_{nano} as the nanotube stochastic strength, i.e. $\sigma_{nano} = 34$ GPa. The computed macrostrength is $\sigma_{macro} = 10.20$ GPa. The fit with Eq. 1 is shown in